Vstx1, a Modifier of Kv Channel Gating, Localizes to the Interfacial Region of Lipid Bilayers†

Daniele Bemporad,‡,§ Zara A. Sands,‡ Chze Ling Wee,‡ Alessandro Grottesi,|| and Mark S. P. Sansom*

Department of Biochemistry, The University of Oxford, South Parks Road, Oxford OX1 3QU, U.K.

Received June 5, 2006; Revised Manuscript Received August 8, 2006

ABSTRACT: VSTx1 is a tarantula venom toxin which binds to the archaebacterial voltage-gated potassium channel KvAP. VSTx1 is thought to access the voltage sensor domain of the channel via the lipid bilayer phase. In order to understand its mode of action and implications for the mechanism of channel activation, it is important to characterize the interactions of VSTx1 with lipid bilayers. Molecular dynamics (MD) simulations (for a total simulation time in excess of 0.2 μs) have been used to explore VSTx1 localization and interactions with zwitterionic (POPC) and with anionic (POPE/POPG) lipid bilayers. In particular, three series of MD simulations have been used to explore the net drift of VSTx1 relative to the center of a bilayer, starting from different locations of the toxin. The preferred location of the toxin is at the membrane/water interface. Although there are differences between POPC and POPE/POPG bilayers, in both cases the toxin forms favorable interactions at the interface, maximizing H-bonding to lipid headgroups and to water molecules while retaining interactions with the hydrophobic core of the bilayer. A 30 ns unrestrained simulation reveals dynamic partitioning of VSTx1 into the interface of a POPC bilayer. The preferential location of VSTx1 at the interface is discussed in the context of Kv channel gating models and provides support for a mode of action in which the toxin interacts with the Kv voltage sensor "paddle" formed by the S3 and S4 helices.

The opening and closing of voltage-dependent cation channels are central to the function of electrically excitable cells, such as neurones and muscle (*1*). Voltage-gated K^+ channels (Kv)[1] are the most intensely studied members of this family (*2*). They are comprised of four identical subunits, with each subunit consisting of six putative α-helices, termed S1−S6, that encircle a central ion conduction pathway. The subunits contain two distinct but functionally coupled domains, namely, the pore domain (S5−S6) and the voltage-sensing (VS) domain (S1−S4), which are responsible for ion conduction and voltage-sensing, respectively.

A variety of peptide toxins derived from the venom of invertebrates such as snakes, scorpions, and spiders are known to inhibit voltage-gated ion channels with a very high affinity (in the 10 nM range) and have proved to be valuable characterization tools (*3*−*6*). These toxins may be classified into two groups based on their mode of action. Pore-blocking toxins target the extracellular pore region and physically occlude the ion conduction pathway (*7*−*18*). In contrast, gating-modifier toxins bind to the VS domain and are thought to alter the conformational changes and energetics of voltage-dependent gating (*19*−*29*).

VSTx1 is an example of a gating-modifier toxin that was isolated from the venom of the *Grammostola spatula* tarantula and has been shown to inhibit the archaebacterial voltage-dependent K^+ channel KvAP (*26*, *27*, *29*, *30*). Although the exact mechanism of inhibition has yet to be fully elucidated, it is known that the binding site must be confined to the VS as the isolated voltage sensor of KvAP is equally as effective at binding VSTx1 as the intact KvAP channel. This strongly suggests that the pore domain of KvAP plays little or no role in the binding of VSTx1. The amino acid sequence of VSTx1 is related to the more fully characterized gating-modifier toxin HATx, which is derived from the venom of the same spider species, and has been shown to inhibit the Kv2.1 channel (*19*, *22*, *23*, *25*, *28*). These toxins share a common structure based upon a cysteine knot motif formed by six highly conserved cysteine residues.

The S4 helix of the VS domain of Kv channels contains a regular array of highly conserved positively charged amino acids (typically arginine), located toward its N-terminus. The S4 helices are believed to move toward the extracellular surface of the membrane in response to membrane depolarization, which ultimately leads to channel activation. The extent of the motion of the S4 helices (and of the VS domains) is the subject of some debate (*31*−*33*). Three X-ray structures of Kv channels are known, and these reveal different orientations of the S4 helices relative to the pore

† This work was supported by funding from the Wellcome Trust and EPSRC (via the Integrative Biology project). The financial support of GlaxoSmithKline for the early stages of this work is gratefully acknowledged.

* To whom correspondence should be addressed: e-mail, mark.sansom@bioch.ox.ac.uk; phone, +44 1865 275371; fax, +44 1865 275373.

‡ These authors contributed equally to this work.

§ Current address: Janssen Pharmaceutica N.V., Belgium.

|| Current address: Consorzio Interuniversitario per le Applicazioni del Supercalcolo per Universita' e Ricerca, Via dei Tizii, 00185 Roma, Italy.

[1] Abbreviations: HATx, hanatoxin; POPC, palmitoyloleoylphosphatidylcholine; POPE, palmitoyloleoylphosphatidylethanolamine; POPG, palmitoyloleoylphosphatidylglycerol; Kv, voltage-gated K^+ channel; VSTx1, tarantula venom toxin.

10.1021/bi061111z CCC: $33.50
Published on Web 09/09/2006

domain of the channel protein. The first X-ray structure of a Kv channel to be determined was that of KvAP, from the archeabacterium *Aeropyrum pernix*, complexed with a monoclonal antibody Fab fragment (*34*). This structure revealed that the S3 helix was distorted into two distinct helical segments, namely, S3a and S3b. The C-terminal S3b segment and the N-terminal portion of S4 (which includes the gating charges) were packed tightly together to form a helix−turn−helix motif, termed a VS paddle. A subsequent structure of KvAP reveals a somewhat different orientation of the VS paddle relative to the pore domain (*35*). The X-ray structure of Kv1.2, a mammalian channel, reveals the S3 and S4 helices to be relatively undistorted and to adopt a presumed transmembrane (TM) orientation (*31*, *36*). This is comparable to the structure observed in crystals of the *isolated* VS domain from KvAP (*34*). From these structural studies it may be suggested that the VS domain possesses a degree of conformational and orientational flexibility. Such flexibility may play a key role in the voltage-sensing function of this domain.

The location and orientation of the VS, and changes in these upon channel activation, have been studied by a number of biophysical techniques (*37*−*50*). For example, introduction of pairs of cysteine residues into S4 and into the pore domain of Shaker Kv channels, combined with Cd^{2+} binding to assess their proximity and molecular modeling (*51*), suggested that S4 adopted a TM orientation (*52*). A similar model based on analysis of structural restraints was used to argue for relatively small changes in the packing of S2, S3, and S4 upon channel activation (*53*). Again, using cross-linking of pairs of cysteine residues, Elliott et al. (*54*) have proposed a model in which S4 adopted a largely TM orientation in both the closed (resting) and open (activated) states.

Several other studies have indicated a relatively small movement of the S4 helix of Shaker Kv channels upon channel activation. If the first Arg of the S4 helix is replaced by a His residue, the mutant channel forms a proton pore when the membrane is hyperpolarized (*55*). This suggests that the intracellular and extracellular solutions contacting S4 must be separated by a narrow barrier that focuses the electrostatic field across a small region. Fluorescence energy transfer experiments between a donor on S4 and an acceptor formed by a lipophilic ion localized at the water/bilayer interface fail to reveal a change in fluorescence upon activation, which suggests that S4 does not translocate substantially across the membrane (*45*). Similarly, luminescence resonance energy transfer between S4 and a scorpion toxin bound to the pore indicates a vertical displacement of S4 of just ∼2 Å (*44*).

However, interpretation of the results from biophysical studies is not unanimous. Studies on KvAP channels measuring avidin accessibility to different length tethered biotins suggest that the VS is highly mobile and that the gating charge Arg residues move ∼15 to ∼20 Å through the membrane to open the pore (*50*, *56*). Furthermore, from analysis of the interaction of hanatoxin (HATx), a toxin which like VSTx1 is located at the lipid/water interface and which is thought to bind to both the closed and open states of the Kv2.1 channel, it has been argued that the VS may traverse "no more than the outer half of the bilayer" during activation of the channel (*57*).

Extensive scanning mutagenesis studies have revealed that HATx binds to three amino acids (I273, F274, and E277) that are localized on the S3 helix of Kv2.1 (*22*). Mutations at equivalent positions on the S3 helices of other channels have also been shown to reduce the affinity of gating-modifier toxins for other Kv channels (*20*, *24*). The residues that influence voltage sensor toxin affinity map onto the S3b component of the voltage sensor paddle in KvAP, and as such the binding site for VSTx1 is likely to be confined to this region. Gating-modifier toxins also share another striking structural characteristic in that one face of the toxin is almost exclusively hydrophobic and thus is likely to partition to the lipid membrane (*27*, *29*). Such a process would be accompanied by a free energy of partitioning which may account for the high apparent toxin binding affinities and moreover would imply that the VS paddle is positioned within the lipid bilayer (*27*).

Molecular modeling and simulations provide a useful tool for examining the interactions of membrane proteins (*58*−*61*). They have been used extensively to model the interactions of Kv channels with pore-blocking toxins (*62*−*69*). More recently, there have been some modeling and simulation studies of HATx (*70*−*73*). In particular, MD simulations have been used to explore the interactions of HATx with a DPPC (dipalmitoylphosphatidylcholine) bilayer (*74*).

In this study, we use MD simulations to explore the preferred location of VSTx1 within both a zwitterionic (POPC, palmitoyloleoylphosphatidylcholine) and a negatively charged (POPE:POPG = 3:1; palmitoyloleoylphosphatidylethanolamine and palmitoyloleoylphosphatidylglycerol) lipid bilayer environment. This is of particular importance as experimental studies suggest some dependence of toxin location on lipid bilayer composition. The results of our simulations cast some light on possible mechanisms of toxin−VS domain interactions.

METHODS

Toxin Structures Used in Simulations. The simulations performed are summarized in Table 1. The simulations of VSTx1 in a POPC bilayer were initiated using a homology model of the toxin built with Modeller 6 (*75*) (http://salilab.org/modeller/modeller.html) using HATx1 [PDB entry 1D1H (*23*)] as the template structure. HATx1 and VSTx1 share a 41% sequence identity and the same pattern of disulfide bridges and were assumed to have the same fold (Figure 1). Since the completion of the VSTx1 in POPC simulations, a solution NMR structure of VSTx1 has been solved by Jung et al. (*29*). Comparison of the homology model of VSTx1 with the NMR structure reveals that both structures share a very similar fold. The only significant differences are at the flexible termini and in two flexible loops. Crucially, the distributions of the hydrophobic and charged residues on the surface of the two structures are also very similar. Separate simulations of the homology model and the NMR structure in water were performed to investigate the validity of the VSTx1 homology model. The toxin model used to initiate simulations of VSTx1 in a POPE/POPG bilayer was derived from the solution NMR structure.

Bilayer Setup. Simulations were performed using both a zwitterionic lipid (POPC) bilayer and a net anionic bilayer (a 3:1 mixture of POPE and POPG). An equilibrated POPC

Table 1: Summary of Simulations[a]

simulation	toxin structure	toxin charges	environment	starting z (Å)
VSTx-PC	model	default	POPC bilayer	0−30.5; restrained
VSTx-ND-PC	model	nondefault	POPC bilayer	0−16.5; restrained
VSTx-PEPG	NMR	default	POPE/POPG 3:1 bilayer	0−30.5; restrained
VSTx-PC-free	model	default	POPC	30.5; 10 ns restrained + 30 ns free
VSTx-W-M	model	default	water	
VSTx-W-N	NMR	default	water	

[a] All simulations were of 10 ns duration, unless stated otherwise. The sets of restrained bilayer simulations were performed at starting z positions of 0, 3, 9.5, 16.5, 23.5, and 30.5 Å. In the default charge simulations all ionizable side chains were fully charged, yielding a net charge of +3 on the toxin. In the ND simulations the net charge was 0 at $z = 0$, 3, and 9.5 Å and +1 at 16.5 Å (see main text for details).

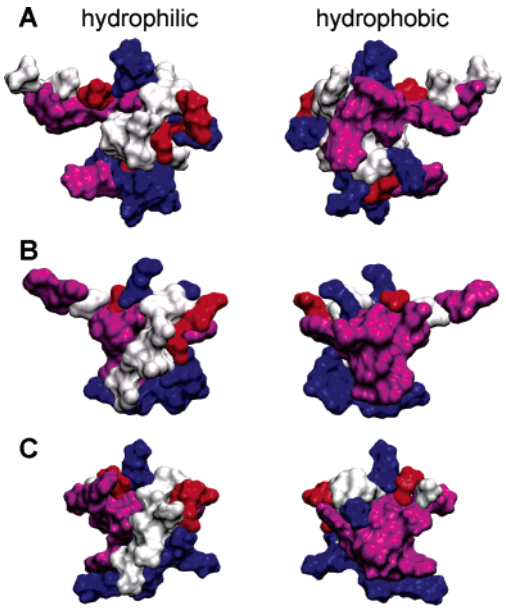

FIGURE 1: Surface residues of HATx1 and VSTx1. Both toxins have a hydrophilic (left) and a hydrophobic (right) face. Basic, acidic, hydrophobic, and polar residues shown in blue, red, purple, and white, respectively. (A) HATx1; (B) VSTx1 homology model; (C) VSTx1 NMR structure.

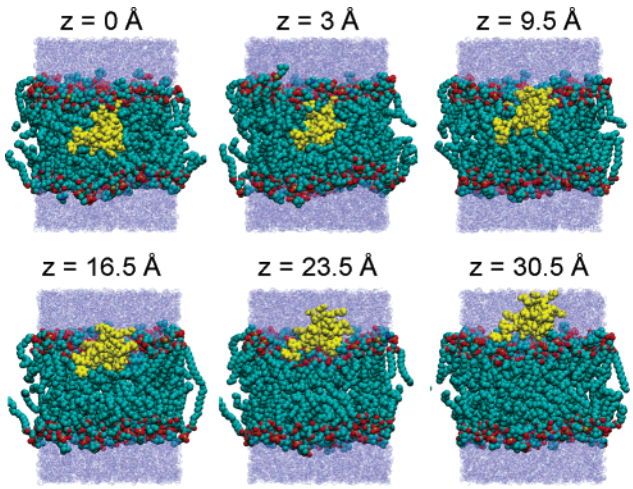

FIGURE 2: Starting depths of the toxin shown for the VSTx1/POPC simulations. The distances of the toxin center of mass from the bilayer center of mass are indicated as z values (the z-axis of the simulation box corresponds to the bilayer normal). VSTx1 is shown in yellow, and POPC carbon, oxygen, nitrogen, and phosphorus atoms are shown in cyan, red, blue, and gold, respectively. The water molecules are shown in light blue.

bilayer comprised of 128 lipid molecules (64 lipid molecules per leaflet) was obtained courtesy of Peter Tieleman (http://moose.bio.ucalgary.ca/). To generate a 3:1 POPE/POPG bilayer, the lipids of the POPC bilayer were converted into POPE and POPG following toxin insertion (see below). To convert a POPC lipid into POPE, each methyl group of the choline of POPC was replaced by a hydrogen atom, followed by a short energy minimization to adjust the N−H bond length. To convert a POPC lipid into POPG, the choline group was replaced with a glycerol group via a least-squared-fitted superimposition.

As the POPG headgroup carries a net negative charge, it was necessary to establish a symmetrical POPE/POPG bilayer while maintaining an even distribution of the two lipid species if the integrity of the membrane were to be maintained over the course of an MD simulation. As random selection of lipids for conversion could not guarantee these requirements, the positions for the POPE and POPG lipids were chosen to avoid POPG clusters. To achieve this, each leaflet of the POPC bilayer was divided into an 8 × 8 grid, with one POPC lipid occupying each grid point. On each row and column, one POPC lipid out of every four was mutated into POPG, and the remaining POPC lipids were mutated into POPE. The resulting bilayer had 48 POPE lipids and 16 POPG lipids per leaflet, giving a POPE/POPG ratio of 3:1.

Simulations Performed. Overall, just over 0.2 μs of simulations was performed, exploring the conformational dynamics of VSTx1 in two different bilayer environments and in an aqueous environment (Table 1). Simulations VSTx-PC and VSTx-PEPG explored the behavior of (fully ionized) VSTx1 as a function of depth of insertion into a lipid bilayer. VSTx-ND-PC (see below) was used to investigate the effect of changing the ionization state of the toxin molecule as a function of depth. VSTx-PC-free was an extended simulation to examine how the toxin behaved if simply "released" at the surface of the bilayer. Finally, VSTx-W-M and VSTx-W-N were two simulations in water, of the homology model and NMR structure of VSTx1, respectively, to examine whether the two starting structures resulted in any significant structural differences.

Toxin Insertion into the Bilayer. VSTx1 was simulated at six different depths in both POPC and POPE/POPG lipid environments (Table 1, Figure 2). The six different starting depths were chosen to correspond to (i) two locations with the toxin completely buried within the hydrophobic core of the bilayer ($z = 0$ and 3 Å, distances being measured from the midpoint of the bilayer along the z-axis which corresponds to the bilayer normal), (ii) two locations with the toxin spanning the hydrophobic core and the headgroup/water interface ($z = 9.5$ and 16.5 Å), and (iii) two locations with

the toxin between the headgroup region and the adjacent aqueous phase ($z = 23.5$ and 30.5 Å).

In order to ensure a realistic conformation of the lipids in response to the presence of VSTx1, we effectively "grew" the toxin, stepwise, in the bilayer. The atomic coordinates of the VSTx1 were scaled by 0.1 while keeping the center of mass at the required depth in the bilayer. The system was energy minimized for 1000 steps using a steepest descent algorithm, neglecting all intramolecular interactions within the toxin. This enabled the lipids to conform gradually to host the toxin. The original atomic coordinates of VSTx1 were then rescaled by a factor of 0.2 while maintaining the lipid coordinates from the previous minimization. This cycle was repeated until the scaling factor reached 1.0. After each scaling factor and subsequent postminimization, if a lipid phosphorus atom was closer than 2.5 Å to any toxin atom, the lipid was considered to overlap the toxin and was removed. For starting depths 9.5, 16.5, and 23.5 Å in either lipid environment, between one and six lipid molecules were removed in total. VSTx1 was inserted with its hydrophobic face pointing toward the membrane core.

Simulation Protocol. Molecular dynamics simulations were performed using GROMACS 3.1.4 (*76*) (www.gromacs.org). A modified version of the GROMOS-87 force field (*77*) was used for the toxin/bilayer simulations. The GROMOS-96 force field (*78*) was used for the VSTx1 in water simulations. Waters were modeled according to the simple point charge (SPC) scheme (*79*). Counterions (Na^+ or Cl^- depending on the system) were added to keep each system electronically neutral. The systems were simulated under periodic boundary conditions (PBC) with each unit cell represented as a rectangular box, with the *xy*-plane and *z*-axis corresponding to the bilayer surface and the bilayer normal, respectively. For the toxin/bilayer systems, the pressures were coupled semiisotropically using the Berendsen barostat at 1 bar with a coupling constant of 1 ps and compressibility value of 4.6×10^{-5} bar^{-1}. For the VSTx1 in water validation study an NVT ensemble was employed; therefore, the systems were not pressure-coupled. The temperatures of the toxin, waters, counterions, and the bilayer (where applicable) were separately coupled using the Berendsen (*80*) thermostat at 300 K, with a weak coupling constant of 0.1 ps. Long-range electrostatic interactions were calculated using the particle mesh Ewald (PME) method (*81*, *82*), employing a grid spacing of ~ 1 $Å^{-1}$ and an interpolation order of 4. A cutoff of 12 Å was used for the real space portion of the Ewald sum and the Lennard-Jones interactions. The LINCS algorithm (*83*) was applied to constrain all covalent bonds, and the SETTLE algorithm (*84*) was used to maintain the geometry of the water molecules. For the toxin/bilayer systems, a harmonic potential with a force constant of 100 kcal mol^{-1} $Å^{-2}$ along the *z*-axis was applied to the toxin center of mass to restrain the toxin at the required depth within the bilayer.

Prior to production, the toxin/bilayer systems were energy minimized using a steepest descent method for 1000 steps. For the toxin/water systems (considered for the validation study), only 100 steps were performed. All systems were then heated from 0 to 300 K, in steps of 50 K. Each step consists of a 10 ps molecular dynamics run, without any restraints applied on the system. The system was then allowed to equilibrate at 300 K for 0.5 ns. Production run simulations were then performed for 10 ns, unless specified otherwise.

All analyses were performed using GROMACS and locally written code. Molecular graphics images were generated using VMD (*85*).

RESULTS

VSTx1 Homology Model vs NMR Structure. Comparison of the surface-exposed residues of the VSTx1 homology model and NMR structure (Figure 1) reveals them to be extremely similar. Both structures were used as initial models for 10 ns simulations in water. The root mean square deviation (rmsd) between the Cα atoms of the time-averaged homology structure and the Cα atoms of the time-averaged NMR structure after a least-squared fit was 0.83 Å, indicating that the structures are virtually indistinguishable. Analysis of a Cα rmsd matrix in which pairwise comparisons are made between all structures in the two simulations reveals that the rmsd for some pairs is as low as ~0.4 Å. In order to evaluate the conformational stability in water of the two VSTx1 structures, we measured the rmsd of the Cα atoms from their starting coordinates. In each case the Cα rmsds fluctuate in the range of ~1 to ~3 Å (data not shown; see Supporting Information, Figure S1). This reveals that both structures undergo a similar degree of structural drift during the course of each simulation. When we consider the rmsd values ignoring the Cα atoms of the first and final two residues (the termini of the toxin move significantly more than the remainder), an even closer correlation is obtained with rmsd values fluctuating between ~0.5 and ~1.5 Å for both simulations. There is no overall drift in rmsd for either simulation, and so we may consider that the toxin structure is conformationally stable in water. The hydrophobic residues remained exposed to water over the 10 ns duration of the simulations.

The relative flexibilities of the homology model and NMR structure were also explored by calculating the root mean square fluctuation (RMSF) of each Cα atom from its starting coordinates. The RMSF plot (Figure 3A) reveals that the flexibility profiles for the two simulations are essentially identical. From a functional point of view, it is also valuable to note that the patterns of average relative solvent-accessible surface areas for the two simulations are almost indistinguishable (Figure 3B). We thus may conclude that the simulated behavior of the homology model and the NMR structure is almost identical.

Toxin Location in the Bilayer. In almost all simulations (Figure 2) there is a degree of displacement of the toxin along the bilayer normal relative to the starting position, despite the harmonic restraint applied to the center of mass of each toxin in the bilayer simulations. This indicates a tendency for the toxin to move toward its equilibrium location of interaction.

To analyze this, we examined distributions of the *z*-coordinate of the center of mass of the toxin (relative to the center of mass of the bilayer) over the simulation period. This corresponds to the displacement of the toxin along the *z*-axis (the bilayer normal). The directionality of movement from the different toxin starting depths for VSTx1 in POPC (Figure 4A) and VSTx1 in POPE/POPG (Figure 4B) suggests a preferred toxin depth of ~16.5 and ~23.5 Å, respectively.

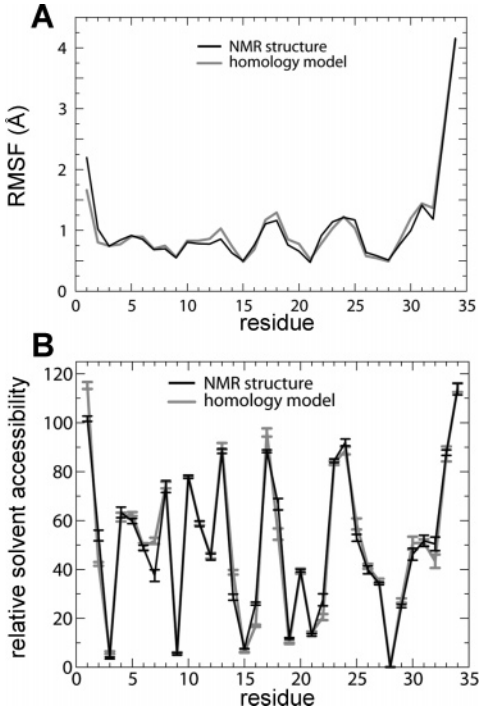

FIGURE 3: Comparisons of the VSTx1 homology model-based and NMR structure-based simulations. (A) RMSF of Cα atoms with respect to the starting coordinates for simulations VSTx-W-N (black line) and VSTx-W-M (gray line). (B) Average relative solvent-accessible surface area (as a percentage; bars represent standard error) for simulations VSTx-W-N (black line) and VSTx-W-M (gray line).

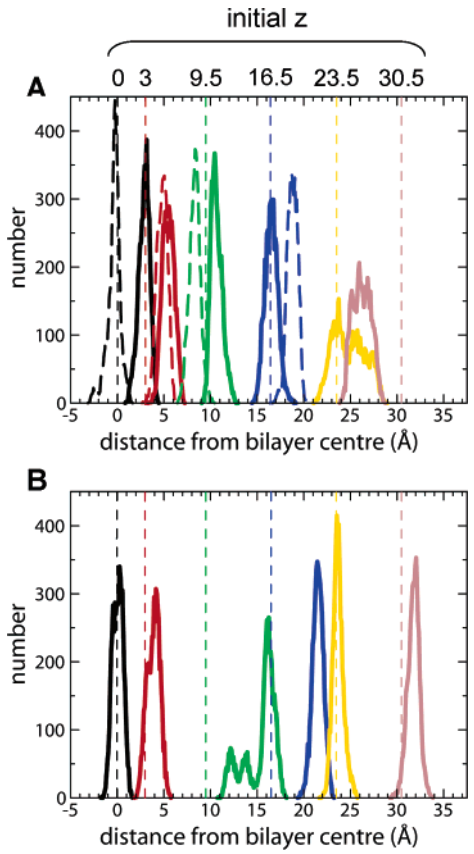

FIGURE 4: Distribution of toxin depths in the bilayer. The labeled vertical broken lines indicate the starting depths for the toxin. (The *z*-axis of the simulation box corresponds to the bilayer normal.) The center of mass of the bilayer was taken to be the reference ($z = 0$ Å). (A) VSTx-PC (solid lines) and VSTx-ND-PC (broken lines); (B) VSTx-PEPG.

The region from 16.5 to 23.5 Å corresponds to the interfacial region (headgroup/water interface) of the bilayer. This proposed location suggests that VSTx1 prefers to be located close to the membrane/water interface, with the toxin orientated such that its hydrophilic face sits in the interfacial region, with its hydrophobic face exposed to the membrane core. From these results, it is also evident that lipid headgroup type plays an instrumental role in determining the preferred toxin depth.

We note that in a couple of cases secondary peaks are seen in the distributions. Analyses of those distributions with secondary peaks (e.g., Figure 4A, VSTx-PC 23.5 Å, and Figure 4B, VSTx-PEPG 9.5 Å) indicated an overall unidirectional movement in *z*, although there are some slight bidirectional fluctuations along the way, probably due to thermal fluctuations.

Sensitivity of the Simulations. In each of the simulations described above, all ionizable side chains of VSTx1 (i.e., E1, K4, K8, K10, D14, K17, D18, R24, and K26) were assumed to be in their fully charged (i.e., default ionization) states, appropriate for pH 7. Given that electrostatic interactions can be expected to play a role in determining the preferred toxin depth within these bilayer environments, one could argue that the assigned protonation states could affect the simulation results. At depths of 23.5 and 30.5 Å, each toxin is exposed to the aqueous environment; therefore, it is not unreasonable to assume that the ionizable side chains will exist in their default states. However, at depths of 0 and 3 Å, the low dielectric environment of the membrane core is likely to suppress side chain ionization. To explore the sensitivity of these simulations to the charge state of the toxin side chains, we repeated the simulations of VSTx1 in POPC at $z = 0$ and 3 Å with all of the ionizable side chains in their neutral states (using the same starting structures and simulation protocols).

Further to this, the toxins located at 9.5 and 16.5 Å span the hydrophobic core and the headgroup/water interface. It is therefore difficult to predict with certainty the likely protonation states of their side chains. To investigate this further, we repeated the simulations of VSTx1 in POPC at these interfacial depths using the nondefault (ND) side chain ionization states predicted using the program WhatIf (*86*) for pK_A calculations, with VSTx1 embedded in a membrane mimetic slab at a depth similar to that in the POPC bilayer. At depths of 9.5 and 16.5 Å, the toxin was assigned an overall charge of 0 (corresponding to E1, K4, K10, D14, D18, and R24 with fully charged side chains) and +1 (E1, K4, K10, D14, D18, R24, and K26 with fully charged side chains), respectively. While the results from these simulations (Figure 4A, broken lines) suggest a degree of sensitivity to side chain ionization states, the overall preferred interfacial location of VSTx1 in POPC is maintained.

Bilayer and Toxin Structures. The integrity of the lipid bilayer during the toxin/bilayer simulations was evaluated by checking that the surface area per lipid molecule remained within the experimental range (*87*). The orientation of the toxin's hydrophobic moment was maintained in all of the simulations (pointing toward the bilayer core), with the angle of the hydrophobic moment fluctuating less than 50° with

respect to the bilayer normal. Note that the hydrophobic moment may be defined as the vector sum of the hydrophobicity of each constituent group of a molecule (*88*) and thus provides a measure of the net magnitude and direction of the hydrophobicity of a toxin. This provides evidence that the natural orientation of VSTx1 in a lipid bilayer is such that its hydrophobic face is pointed toward the membrane core. In this orientation, the basic residues of VSTx1 are located in the interfacial region, close to the headgroup region of the bilayer.

The integrity of the VSTx1 structure was monitored by analyzing the rmsd of the Cα atoms as a function of time with respect to the starting coordinates. Across the simulations, the rmsd for VSTx1 fluctuated in the range of ~1.25 to ~3.5 Å (see Supporting Information, Figure S2), which indicates a degree of distortion in the toxin structure, but in no case did the toxin unfold. We also examined the root mean square fluctuations (RMSFs) in the toxin structures (see Supporting Information, Figure S3). It was found that the C- and N-termini of VSTx1 exhibited the highest degree of flexibility with RMSF values of up to ~3.5 Å. The overall pattern of flexibility along the length of the toxin mirrors the presence of secondary structure elements and disulfide bridges in the toxin. Two low RMSF zones extending from residues 19 to 22 and residues 27 to 29 are observed which correspond with the two β-strands. A low RMSF region centered about residue 15 is also seen, which is consistent with the short 3_{10} helix. Finally, the zone extending from residues 2 to 9 corresponds to Cys2 and Cys9, that form disulfide bridges which severely restrict the mobility of the protein.

Electrostatic Interactions. To better understand the factors that determine the preferred toxin depth, we investigated the electrostatic interactions between the toxin and the lipid molecules of the bilayer. We examined the atomic (number) densities along the bilayer normal for the charged components of the simulation systems, averaged over the simulation period. For VSTx1 in POPC (Figure 5A), VSTx1 in POPE/POPG (Figure 5B), and VSTx1-ND in POPC simulations (data not shown), at the average (over the simulation period) toxin depths closest to the preferred toxin depths (~16.5, ~23.5, and ~23.5 Å, respectively), there is a high degree of overlap between (i) the basic residues of the toxin and of the phosphate groups of the lipid molecules and (ii) the acidic residues of the toxin and the choline of POPC and the ethanolamine of POPE.

We also analyzed the number of contacts between the six basic residues of VSTx1 (K4, K8, K10, K17, R24, and K26) with the phosphate groups of POPC for VSTx1 in POPC (data not shown). The general trend is that for aqueous (z = 23.5 and 30.5 Å) or interfacial (z = 16.5 Å) locations the number of contacts increases significantly over time. This suggests that the toxin interacts with the membrane in such a way as to maximize (to the extent possible over the time scale of the simulations) the number of electrostatic interactions of its basic side chains with the phosphates of the lipid headgroups.

Taken together, these results suggest that (i) electrostatic interactions are likely to play a key role in stabilizing the toxin at a particular depth within a lipid bilayer, (ii) the dominant electrostatic interactions appear to be between the basic residues of the toxin and the phosphate group of the lipid molecules, and (iii) the phosphate groups of the two lipid species in the POPE/POPG lipid bilayer are displaced to larger z values relative to their POPC counterparts.

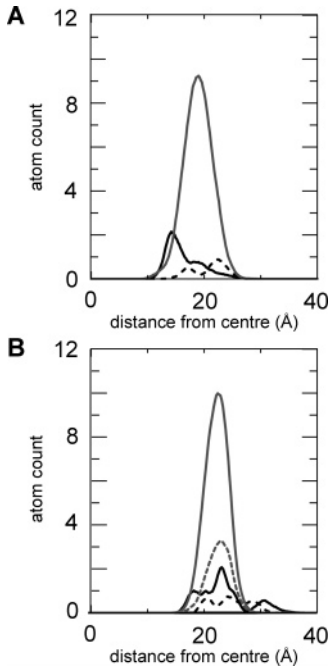

FIGURE 5: Distribution of lipid headgroup and toxin charged groups at the membrane/water interface for simulations (A) VSTx-PC z = 16.5 Å and (B) VSTx-PEPG z = 23.5 Å. Distributions for basic (solid black line) and acidic (broken black line) residues of the toxin are shown, along with those of the phosphate group [gray lines; in (A) for all phosphates, in (B) for the POPE (solid) and POPG (broken) phosphate separately].

H-Bonding. H-bonding is also expected to play a role in stabilizing the toxin at a particular depth relative to the bilayer. VSTx1 is capable of forming H-bonds with the phosphate and carbonyl groups of POPC, POPE, and POPG and with the ethanolamine group of POPE and the glycerol group of POPG. In Figure 6 we display the variation in the number of H-bonds for VSTx1 in POPC and VSTx1 in POPE/POPG over the simulation period for the initial z = 16.5 Å simulations. (The H-bonding results for VSTx1-ND in POPC are similar to these two systems and are not shown.) It can be seen (e.g., Figure 6A) that the number of H-bonds with phosphate groups is still increasing after 10 ns. Such nonequilibrium features are, in part, due to the limited time scale of the simulations. However, they do not alter the main conclusions of the H-bond analysis.

In particular, over time we see a gradual decline in the number of toxin−water H-bonds (not shown) in favor of an increase in toxin−lipid H-bonds, especially H-bonds between the toxin and the phosphates of the lipid headgroups. Thus, the toxin−lipid interactions are optimized during the course of each simulation. The number of H-bonds of the toxins with the different groups of the lipid moieties (phosphate, carbonyl, ethanolamine, and head glycerol) varies with toxin depth in a manner which corresponds to the location of each group along the vertically aligned lipid molecules. At the preferred toxin depth of 23.5 Å for VSTx1 in POPE/POPG although the toxin forms a large total number of H-bonds, it does not correspond to the maximum total number of H-bonds (Figure 7). This is also true for the other systems and suggests that although H-bonding plays a role in

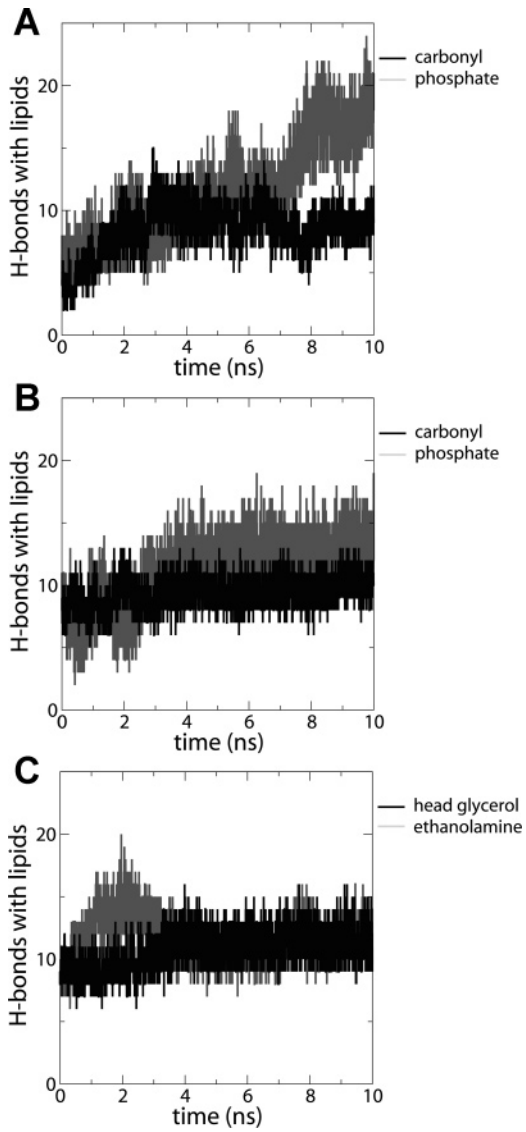

FIGURE 6: H-bonds with lipid as a function of time for the initial $z = 16.5$ Å simulations: (A) VSTx-PC and (B, C) VSTx-PEPG. In (A, B) the black line shows H-bonds between the toxin and carbonyl oxygens of the lipid, whereas the gray line shows H-bonds between the toxin and lipid phosphates. In (C) the black line shows H-bonds between the toxin and headgroup glycerol groups of POPG, whereas the gray line shows H-bonds between the toxin and headgroup ethanolamine groups of POPE.

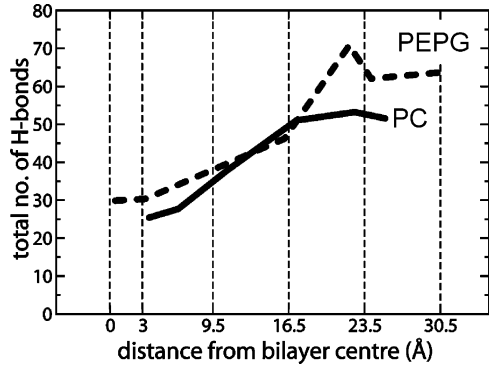

FIGURE 7: The average total number of H-bonds versus the average toxin depth for the final 1 ns of simulation VSTx-PC (solid line) and VSTx-PEPG (broken line).

stabilizing the toxin at a particular depth, it is probably not the only factor in determining the overall toxin location. As

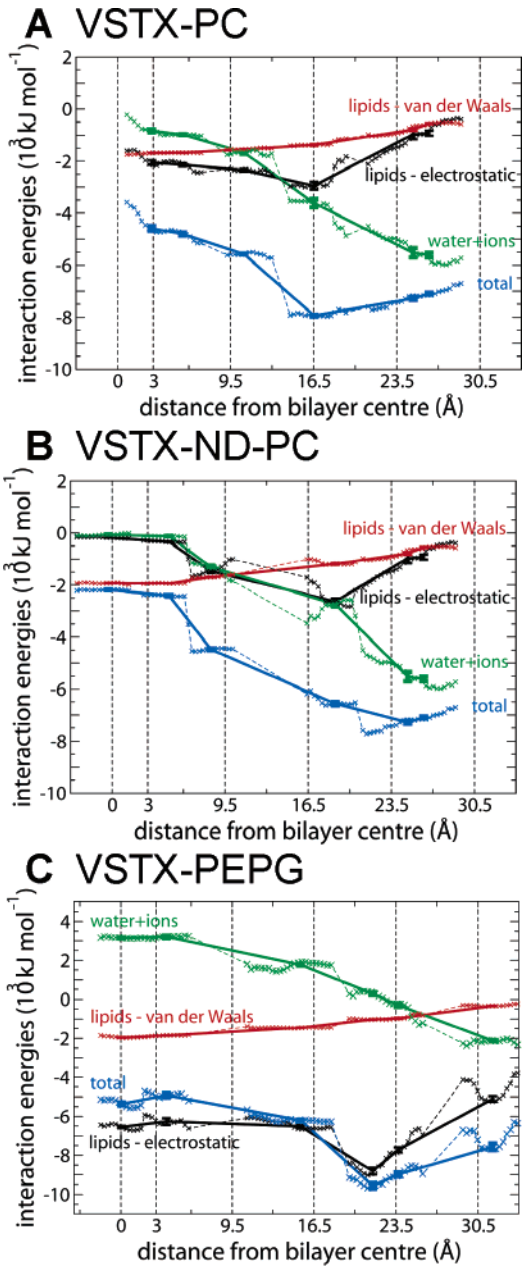

FIGURE 8: Toxin−environment interaction energies as a function of toxin depth for simulations: (A) VSTx-PC, (B) VSTx-ND-PC, and (C) VSTx-PEPG. The solid lines indicate average interaction energies vs average toxin depth over the entire simulation period, whereas the dotted lines provide a more detailed view of the energetics.

z increases, the number of toxin−water H-bonds increases (data not shown). It is apparent that water molecules can penetrate the interfacial region of the bilayer. Indeed, at the higher toxin depths (16.5, 23.5, and 30.5 Å), the total number of H-bonds is dominated by the toxin−water H-bonding term.

Interaction Energies. The toxin is expected to prefer a location at which its interaction energy with its environment (i.e., both lipids and water molecules) is at a minimum. We therefore investigated the interaction (potential) energies between the toxin and its environment for each simulation. The interaction energies as a function of z-depth over the course of each simulation (Figure 8) were decomposed into two components, namely, the toxin−lipid and toxin−solvent

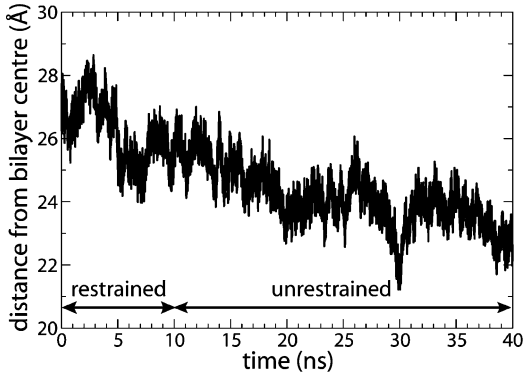

FIGURE 9: Trajectory of the toxin along the *z*-axis for simulation VSTx-PC-free. The simulation starts with the toxin at $z = 30.5$ Å (which corresponds to the toxin sitting just on the bilayer surface). The toxin was restrained from $t = 0-10$ ns, and then from $t = 10-40$ ns the restraint was removed.

(i.e., water and counterions) interaction energies. The toxin−lipid interaction energy term was further decomposed into the contributions arising from electrostatic and from van der Waals interactions. The earlier distribution analyses (Figure 4) indicated preferred toxin depths of ∼16.5, ∼23.5, and ∼23.5 Å for VSTx1 in POPC, VSTx1-ND in POPC, and VSTx1 in POPE/POPG, respectively. In each case, this preferred depth corresponds to an overall minimum in the total interaction energy profile.

For the toxin in POPC simulations, the total interaction energy profiles (Figure 8AB) appear to be dictated by a combination of the toxin−solvent interaction energy and the electrostatic component of the toxin−lipid interaction. Interestingly, the total interaction energy profile for VSTx1 in POPE/POPG (Figure 8C) appears to be dominated by the electrostatic component of the toxin−lipid contribution. These results indicate that the nature of the lipid headgroup has a strong influence on toxin partitioning, as is observed experimentally.

Toxin Partitioning and Interactions with the Voltage Sensor Domain. It has been suggested (*26*, *27*, *29*) that VSTx1 reaches its target (the voltage-sensing paddle of KvAP) by dynamically partitioning into anionic headgroup lipid membranes. However, there is still some discussion over whether or not VSTx1 can partition into a *zwitterionic*, POPC, bilayer. To explore this further, we extended the simulation of VSTx1 in POPC at 30.5 Å (this corresponds to the toxin sitting on the surface of the bilayer) for a further 30 ns, with the harmonic restraint no longer applied. With the positional restraint removed from VSTx1 the toxin does indeed dynamically partition into the bilayer (Figure 9) such that after 40 ns the toxin reached a depth of $z = \sim 22.5$ Å. This depth corresponds to the more hydrophobic half of the toxin penetrating the headgroup and acyl tail regions of the bilayer, supporting the notion that dynamic partitioning of VSTx1 does occur in a POPC bilayer.

Mutational studies to probe the interactions of voltage sensor binding toxins with Kv channels (*26*−*28*) point to an interaction between polar/charged and hydrophobic residues on the toxin surface with residues toward the C-terminus of the S3b helix of the voltage sensor. On the basis of this information we can model the positions of VSTx1 and the KvAP voltage sensor relative to a POPC lipid bilayer. Thus, as seen in Figure 10, VSTx1 is located

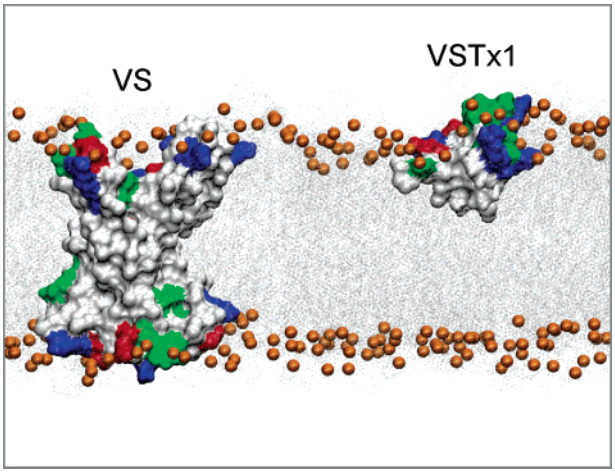

FIGURE 10: Comparison of the preferred localizations in a POPC bilayer of VSTx1 (right) and the voltage sensor domain of KvAP (PDB code 1ORS). The snapshot of the KvAP VS domain is taken from the end of a 50 ns MD simulation performed in POPC (Sands, Grottesi, and Sansom, manuscript in preparation). This is shown alongside the final snapshot from the VSTx-PC simulation starting at $z = 16.5$ Å. The surface of the VS and toxin are shown with hydrophobic, polar, positive, and negative residues depicted in white, green, blue, and red, respectively. The POPC lipids are represented in gray, with the phosphorus atoms of the headgroups shown as orange spheres.

such that its center of mass is ∼15 Å away from the central plane of the bilayer. This places the toxin with a band of positively charged residues (which are likely to form the interactions between the toxin and the voltage sensor) exactly at the interface. The KvAP voltage sensor crystal structure (i.e., that of the isolated voltage sensor domain, PDB code 1ORS) may be positioned in a POPC bilayer such that (i) it spans the bilayer symmetrically and (ii) the surface-exposed tyrosine (Y46 of S1) is at the interface [tyrosine and tryptophan residues tend to be located in bands on the surfaces of membrane proteins corresponding to the lipid/water interface (*89*)]. In this orientation, which is supported by MD simulations of the voltage sensor domain in a bilayer (Sands and Sansom, manuscript in preparation), the residues in the S3b helix are aligned at just the right depth to interact with the basic residues of VSTx1. This would support a location of the tip of the gating paddle at the extracellular interfacial region of the membrane, at least when KvAP is in a conformation able to bind VSTx1. It is suggested that the interaction of VSTx1 and KvAP requires depolarization of the membrane (*56*), suggesting that the VSTx1 binding state of KvAP may correspond to an open/activated state of the channel.

DISCUSSION

We have performed a series of MD simulations (corresponding to a total simulation time of >0.2 μs) and embraced two different lipid bilayer environments to reveal the preferred location of VSTx1 in zwitterionic and in negatively charged membranes. The principle outcome of this study is that VSTx1 is preferentially located at the lipid/water interface, in either a zwitterionic or an anionic lipid bilayer environment. Its hydrophobic residues point toward the hydrophobic core of the bilayer, and its hydrophilic residues interact with lipid headgroups and water molecules. Electrostatic interactions between charged side chains on the

surface of the toxin and the phosphate groups of the lipid molecules play a key role in determining the location of the toxin.

These results, and especially the difference in toxin location, are of interest in the context of experimental data on VSTx1−bilayer interactions. Lee and MacKinnon suggested that VSTx1 interacts equally well with anionic and zwitterionic phospholipids (*27*). In contrast, Jung et al. indicated that the interaction of VSTx1 with membranes requires the presence of anionic phospholipids (*29*). Our simulations reveal the dynamic molecular process of VSTx1 partitioning into a zwitterioninc POPC bilayer, thus supporting the contention that VSTx1 does in fact partition into neutral phospholipid bilayers. However, our simulations also indicate that, at the preferred toxin interaction depth, there is a greater potential energy of interaction of VSTx1 with POPE/POPG over POPC.

The simulations also reveal that the preferred location of VSTx1 in the anionic POPE/POPG bilayer is largely dictated by favorable electrostatic interactions between the toxin and the lipid headgroups. Although electrostatic interactions between the toxin and lipid headgroups play a role in stabilizing VSTx1 in the neutral POPC environment, it is found that favorable interactions between the toxin and water molecules that penetrate the interface also play a role in determining the preferred toxin location. Intriguingly, at the putative preferred toxin depths, optimal overlap between the charged residues of the toxin and the charged components of the lipid bilayer occurs. This may help to rationalize the preferred toxin locations.

It is interesting to compare our simulation results with those of a recent study of the interactions of HATx with a DPPC bilayer (*74*). These simulations also indicated that the toxin preferred to be located at the bilayer/water interface, although some degree of local bilayer distortion was also observed. It should be noted that HATx is thought to bind to both the closed and open states of Kv2.1, whereas VSTx1 is suggested to bind to the open state of KvAP (see discussions in, e.g., refs *26*, *27*, *50*, *56*, and *57*). Hence, one might expect them to partition to slightly different locations. In this context, it would be of interest to simulate a number of gating-modifier toxins (VSTx1, HATx, SGTx) in both zwitterionic and anionic lipid bilayers to examine further details of differences in toxin−bilayer interactions, which in turn may help to inform our understanding of voltage-sensing mechanisms by Kv channels.

Mutational studies on voltage sensor binding toxins combined with mutational studies of Kv channels point to an interaction between polar/charged and hydrophobic residues on the toxin surface with the residues toward the C-terminus of the S3b helix of the voltage sensor paddle (*90*). Additional studies of VSTx1 interactions with KvAP suggest that membrane depolarization (i.e., a switch from a resting to an open/activated state) is required for the toxin and the voltage sensor to interact (*56*). Therefore, the preferential partitioning of VSTx1 into the water/lipid interface suggests that the *activated* VS paddle is localized in this region, too. Given that the preferred toxin locations differ when VSTx1 partitions into a POPC or a POPE/POPG environment, it is possible that the lipid environment may also influence the nature of the toxin−VS interaction and/or that the conformation of the VS is sensitive to the lipid environment (*35*). As comparison of crystal structures suggests a degree of flexibility in VS−pore interactions, this may be of functional importance.

In addition to insights into some of the complexities of toxin−phospholipid interactions, the current simulations may also be used as a starting point for modeling the interaction of VSTx1 with the VS of KvAP (Figure 10). In particular, simulations of both components individually in lipid bilayers provide ensembles of structures for subsequent docking studies.

It is important to consider possible methodological limitations of the current studies. As discussed above, one assumption is the assignment of fixed ionization states to toxin side chains. Given the role that electrostatic interactions play in determining the preferred toxin depths within these lipid bilayer environments, it is likely that the assigned side chain ionization states could influence toxin partitioning. We have attempted to explore the sensitivity to such assumptions. However, in the future it may be possible to reassign ionization states dynamically during the course of a simulation (*91*).

Also, in the context of the treatment of electrostatics, we note that the concentrations of counterions may influence toxin−bilayer interactions. Each simulation system has on average ∼5000 water molecules. The systems with the most counterions are the VSTx-PEPG simulations because of the anionic POPG lipid molecules. The VSTx-PEPG systems had 29 Na^+ counterions each, giving a Na^+ concentration of ∼300 mM. For the zwitterionic system the ionic strength is close to zero. Thus, although there is a difference, even the highest ionic strength is not too high, and we would not expect a significant difference. However, a systematic study of toxin interactions versus ionic strength would be of interest in the future.

A further limitation, especially in the possible extension of these studies to VS−toxin interactions, is the limited time scale of the simulations. Due to the computational expense of performing all-atom MD simulations for complex biological systems, simulation times are typically limited to tens of nanoseconds. Inevitably, this means that we cannot observe phenomena that occur over longer time scales, e.g., dynamic toxin partitioning into a lipid bilayer. Such limitations should always be borne in mind when considering data derived from nonequilibrated processes. With respect to our study, we would therefore not expect to see convergence of the POPC and POPE/POPG series of simulations; however, finite time scales do offer the advantage of allowing us to probe the dynamic response between the lipid bilayer and the toxin positioned at a variety of depths. From the analysis we performed, we do observe clear trends in the experimental data that offer a detailed qualitative insight into the processes that govern toxin partitioning. Recent advances in coarse-grained simulations (*92*) and their application to membrane proteins (*93*, *94*) offer a possible route to extended (∼1 μs) simulations of channel−toxin interactions. Coarse-grained simulations also offer the possibility of a definitive toxin location via free energy calculations. Only by calculating a free energy profile (i.e., potential of mean force) for VSTx1 relative to a bilayer may we obtain a definitive quantitative description of toxin partitioning. [Recent studies on the free energy of dimerization of the glycophorin transmembrane domain are promising is this respect (*95*).] However, the

current studies enable an initial approach to the problem of toxin location via estimation of potential energies of toxin−bilayer and toxin−water interactions.

ACKNOWLEDGMENT

Many thanks to all of our colleagues for their interest in this work, especially Frank Blaney and David Gavaghan.

SUPPORTING INFORMATION AVAILABLE

Three figures as described in the text. This material is available free of charge via the Internet at http://pubs.acs.org.

REFERENCES

1. Hille, B. (2001) *Ionic Channels of Excitable Membranes*, 3rd ed., Sinauer Associates Inc., Sunderland, MA.
2. Yellen, G. (2002) The voltage-gated potassium channels and their relatives, *Nature 419*, 35−42.
3. Miller, C. (1995) The charybdotoxin family of K^+ channel-blocking peptides, *Neuron 15*, 5−10.
4. Possani, L. D., Merino, E., Corona, M., Bolivar, F., and Becerril, B. (2000) Peptides and genes coding for scorpion toxins that affect ion channels, *Biochimie 82*, 861−868.
5. Cestele, S., and Catterall, W. A. (2000) Molecular mechanisms of neurotoxin action on voltage-gated sodium channels, *Biochimie 82*, 883−892.
6. de la Vega, R. C. R., and Possani, L. D. (2004) Current views on scorpion toxins specific for K^+-channels, *Toxicon 43*, 865−875.
7. MacKinnon, R., Heginbotham, L., and Abramson, T. (1990) Mapping the receptor site for charybdotoxin, a pore-blocking potassium channel inhibitor, *Neuron 5*, 767−771.
8. Bontems, F., Roumestand, C., Gilquin, B., Menez, A., and Toma, F. (1991) Refined structure of charybdotoxin—common motifs in scorpion toxins and insect defensins, *Science 254*, 1521−1523.
9. Bontems, F., Gilquin, B., Roumestand, C., Menez, A., and Toma, F. (1992) Analysis of side-chain organization on a refined model of charybdotoxin: structural and functional implications, *Biochemistry 31*, 7756−7764.
10. Goldstein, S. A. N., Pheasant, D. J., and Miller, C. (1994) The charybdotoxin receptor of a Shaker K^+ channel: peptide and channel residues mediating molecular recognition, *Neuron 12*, 1377−1388.
11. Krezel, A. M., Kasibhatla, C., Hidalgo, P., Mackinnon, R., and Wagner, G. (1995) Solution structure of the potassium channel inhibitor agitoxin-2−caliper for probing channel geometry, *Protein Sci. 4*, 1478−1489.
12. Gross, A., and MacKinnon, R. (1996) Agitoxin footprinting the Shaker potassium channel pore, *Neuron 16*, 399−406.
13. Naranjo, D., and Miller, C. (1996) A strongly interacting pair of residues on the contact surface of charybdotoxin and a Shaker K^+ channel, *Neuron 16*, 123−130.
14. Savarin, P., Guenneugues, M., Gilquin, B., Lamthanh, H., Gasparini, S., Zinn-Justin, S., and Menez, A. (1998) Three-dimensional structure of kappa-conotoxin PVIIA, a novel potassium channel-blocking toxin from cone snails, *Biochemistry 37*, 5407−5416.
15. Shon, K. J., Stocker, M., Terlau, H., Stuhmer, W., Jacobsen, R., Walker, C., Grilley, M., Watkins, M., Hillyard, D. R., Gray, W. R., and Olivera, B. M. (1998) kappa-conotoxin PVIIA is a peptide inhibiting the Shaker K^+ channel, *J. Biol. Chem. 273*, 33−38.
16. Batista, C. V. F., Gòmez-Lagunas, F., Lucas, S., and Possani, L. D. (2000) Tc1, from Tityus cambridgei, is the first member of a new subfamily of scorpion toxin that blocks K^+-channels, *FEBS Lett. 486*, 117−120.
17. Eriksson, M. A. L., and Roux, B. (2002) Modeling the structure of agitoxin in complex with the Shaker K^+ channel, *Biophys. J. 83*, 2595−2609.
18. Naranjo, D. (2002) Inhibition of single Shaker K channels by kappa-conotoxin-PVIIA, *Biophys. J. 82*, 3003−3011.
19. Swartz, K. J., and Mackinnon, R. (1995) An inhibitor of the Kv2.1 potassium channel isolated from the venom of a Chilean tarantula, *Neuron 15*, 941−949.
20. Li-Smerin, Y., and Swartz, K. J. (1998) Gating modifier toxins reveal a conserved structural motif in voltage-gated Ca^{2+} and K^+ channels, *Proc. Natl. Acad. Sci. U.S.A. 95*, 8585−8589.
21. Cestele, S., Qu, Y. S., Rogers, J. C., Rochat, H., Scheuer, T., and Catterall, W. A. (1998) Voltage sensor-trapping: Enhanced activation of sodium channels by beta-scorpion toxin bound to the S3-S4 loop in domain II, *Neuron 21*, 919−931.
22. Li-Smerin, Y., and Swartz, K. J. (2000) Localization and molecular determinants of the hanatoxin receptors on the voltage-sensing domains of a K^+ channel, *J. Gen. Physiol. 115*, 673−684.
23. Takahashi, H., Kim, J. I., Min, H. J., Sato, K., Swartz, K. J., and Shimada, I. (2000) Solution structure of hanatoxin1, a gating modifier of voltage-dependent K^+ channels: Common surface features of gating modifier toxins, *J. Mol. Biol. 297*, 771−780.
24. Winterfield, J. R., and Swartz, K. J. (2000) A hot spot for the interaction of gating modifier toxins with voltage-dependent ion channels, *J. Gen. Physiol. 116*, 637−644.
25. Lou, K. L., Huang, P. T., Shiau, Y. S., Liaw, Y. C., Shiau, Y. Y., and Liou, H. H. (2003) A possible molecular mechanism of hanatoxin binding-modified gating in voltage-gated K^+-channels, *J. Mol. Recognit. 16*, 392−395.
26. Ruta, V., and MacKinnon, R. (2004) Localization of the voltage-sensor toxin receptor on KvAP, *Biochemistry 43*, 10071−10079.
27. Lee, S. Y., and MacKinnon, R. (2004) A membrane-access mechanism of ion channel inhibition by voltage sensor toxins from spider venom, *Nature 430*, 232−235.
28. Lee, H. C., Wang, J. M., and Swartz, K. J. (2004) Interaction between extracellular hanatoxin and the resting conformation of the voltage-sensor paddle in Kv channels, *Neuron 40*, 527−536.
29. Jung, H. J., Lee, J. Y., Kim, S. H., Eu, Y. J., Shin, S. Y., Milescu, M., Swartz, K. J., and Kim, J. I. (2005) Solution structure and lipid membrane partitioning of VSTx1, an inhibitor of the KvAP potassium channel, *Biochemistry 44*, 6015−6023.
30. Ruta, V., Jiang, Y. X., Lee, A., Chen, J. Y., and MacKinnon, R. (2003) Functional analysis of an archaebacterial voltage-dependent K^+ channel, *Nature 422*, 180−185.
31. Long, S. B., Campbell, E. B., and MacKinnon, R. (2005) Voltage sensor of Kv1.2: structural basis of electromechanical coupling, *Science 309*, 903−908.
32. Freites, J. A., Tobias, D. J., von Heijne, G., and White, S. H. (2005) Interface connections of a transmembrane voltage sensor, *Proc. Natl. Acad. Sci. U.S.A. 102*, 15059−15064.
33. Swartz, K. J. (2004) Towards a structural view of gating in potassium channels, *Nat. Rev. Neurosci. 5*, 905−916.
34. Jiang, Y., Lee, A., Chen, J., Ruta, V., Cadene, M., Chait, B. T., and Mackinnon, R. (2003) X-ray structure of a voltage-dependent K^+ channel, *Nature 423*, 33−41.
35. Lee, S. Y., Lee, A., Chen, J., and MacKinnon, R. (2005) Structure of the KvAP voltage-dependent K^+ channel and its dependence on the lipid membrane, *Proc. Natl. Acad. Sci. U.S.A. 102*, 15441−15446.
36. Long, S. B., Campbell, E. B., and MacKinnon, R. (2005) Crystal structure of a mammalian voltage-dependent Shaker family K^+ channel, *Science 309*, 897−902.
37. Yellen, G. (1998) The moving parts of voltage-gated ion channels, *Q. Rev. Biophys. 31*, 239−295.
38. Bezanilla, F. (2000) The voltage sensor in voltage-dependent ion channels, *Physiol. Rev. 80*, 555−592.
39. Gandhi, C. C., and Isacoff, E. Y. (2002) Molecular models of voltage sensing, *J. Gen. Physiol. 120*, 455−463.
40. Yang, N., and Horn, R. (1995) Evidence for voltage-dependent S4 movement in sodium channels, *Neuron 15*, 213−218.
41. Yang, N. B., George, A. L., and Horn, R. (1996) Molecular basis of charge movement in voltage-gated sodium channels, *Neuron 16*, 113−122.
42. Cha, A., Snyder, G. E., Selvin, P. R., and Bezanilla, F. (1999) Atomic scale movement of the voltage-sensing region in a potassium channel measured via spectroscopy, *Nature 402*, 809−813.
43. Glauner, K. S., Mannuzzau, L. M., Gandhi, C. S., and Isacoff, E. Y. (1999) Spectroscopic mapping of voltage sensor movement in the Shaker potassium channel, *Nature 402*, 813−817.
44. Posson, D. J., Ge, P., Miller, C., Bezanilla, F., and Selvin, P. R. (2005) Small vertical movement of a K^+ channel voltage sensor measured with luminescence energy transfer, *Nature 436*, 848−851.
45. Chanda, B., Asamoah, O. K., Blunck, R., Roux, B., and Bezanilla, F. (2005) Gating charge displacement in voltage-gated ion channels involves limited transmembrane movement, *Nature 436*, 852−856.

46. Larsson, H. P., Baker, O. S., Dhillon, D. S., and Isacoff, E. Y. (1996) Transmembrane movement of the Shaker K^+ channel S4, *Neuron 16*, 387−397.
47. Mannuzzu, L. M., Moronne, M. M., and Isacoff, E. Y. (1996) Direct physical measure of conformational rearrangement underlying potassium channel gating, *Science 271*, 213−216.
48. Yusaf, S. P., Wray, D., and Sivaprasadarao, A. (1996) Measurement of the movement of the S4 segment during the activation of a voltage-gated potassium channel, *Pfluegers Arch. 433*, 91−97.
49. Baker, O. S., Larsson, H. P., Mannuzzu, L. M., and Isacoff, E. Y. (1998) Three transmembrane conformations and sequence-dependent displacement of the S4 domain in Shaker K^+ channel gating, *Neuron 20*, 1283−1294.
50. Ruta, V., Chen, J., and MacKinnon, R. (2005) Calibrated measurement of gating-charge arginine displacement in the KvAP voltage-dependent K^+ channel, *Cell 123*, 463−475.
51. Lainé, M., Lin, M. A., Bannister, J. P. A., Silverman, W. R., Mock, A. F., Roux, B., and Papazian, D. M. (2003) Atomic proximity between S4 segment and pore domain in Shaker potassium channels, *Neuron 39*, 467−481.
52. Lainé, M., Papazian, D. M., and Roux, B. (2004) Critical assessment of a proposed model of Shaker, *FEBS Lett. 564*, 257−263.
53. Silverman, W. R., Roux, B., and Papazian, D. M. (2003) Structural basis of two-stage voltage-dependent activation in K^+ channels, *Proc. Natl. Acad. Sci. U.S.A. 100*, 2935−2940.
54. Elliott, D. J. S., Neale, E. J., Aziz, Q., Dunham, J. P., Munsey, T. S., Hunter, M., and Sivaprasadarao, A. (2004) Molecular mechanism of voltage sensor movements in a potassium channel, *EMBO J. 23*, 4717−4726.
55. Starace, D. M., and Bezanilla, F. (2004) A proton pore in a potassium channel voltage sensor reveals a focused electric field, *Nature 427*, 548−553.
56. Jiang, Y., Ruta, V., Chen, J., Lee, A. G., and Mackinnon, R. (2003) The principle of gating charge movement in a voltage-dependent K^+ channel, *Nature 423*, 42−48.
57. Phillips, L. R., Milescu, M., Li-Smerin, Y., Midell, J. A., Kim, J. I., and Swartz, K. J. (2005) Voltage-sensor activation with a tarantula-toxin as cargo, *Nature 436*, 857−860.
58. Ash, W. L., Zlomislic, M. R., Oloo, E. O., and Tieleman, D. P. (2004) Computer simulations of membrane proteins, *Biochim. Biophys. Acta 1666*, 158−189.
59. Roux, B., and Schulten, K. (2004) Computational studies of membrane channels, *Structure 12*, 1343−1351.
60. Sansom, M. S. P., Bond, P. J., Deol, S. D., Grottesi, A., Haider, S., and Sands, Z. A. (2005) Molecular simulations and lipid/protein interactions: potassium channels and other membrane proteins, *Biochem. Soc. Trans. 33*, 916−920.
61. Deol, S. S., Domene, C., Bond, P. J., and Sansom, M. S. P. (2006) Anionic phospholipids interactions with the potassium channel KcsA: simulation studies, *Biophys. J. 90*, 822−830.
62. Yao, J., Chen, X., Li, H., Zhou, Y., Yao, L. J., Wu, G., Chen, X., Zhang, N. X., Zhou, Z., Xu, T., and Wu, H. M. (2005) BmP09, a "long chain" scorpion peptide blocker of BK channels, *J. Biol. Chem. 280*, 14819−14828.
63. Wang, Y. F., Chen, X., Zhang, N. X., Wu, G., and Wu, H. M. (2005) The solution structure of BmTx3B, a member of the scorpion toxin subfamily alpha-KTx 16, *Proteins: Struct., Funct., Bioinf. 58*, 489−497.
64. Yu, K. Q., Fu, W., Liu, H., Luo, X. M., Chen, K. X., Ding, J. P., and Shen, J. H. (2004) Computational simulations of interactions of scorpion toxins with the voltage-gated potassium ion channel, *Biophys. J. 86*, 3542−3555.
65. Wu, Y. L., Cao, Z. J., Yi, H., Jiang, D. H., Mao, X., Liu, H., and Li, W. X. (2004) Simulation of the interaction between ScyTx and small conductance calcium-activated potassium channel by docking and MM-PBSA, *Biophys. J. 87*, 105−112.
66. Fu, W., Cui, M., Briggs, J. M., Huang, X., Xiong, B., Zhang, Y., Luo, X., Shen, J., Ji, R., Jiang, H., and Chen, K. (2002) Brownian dynamics simulations of the recognition of the scorpion toxin maurotoxin with the voltage-gated potassium ion channels, *Biophys. J. 83*, 2370−2385.
67. Cui, M., Shen, J., Briggs, J. M., Fu, W., Wu, J., Zhang, Y., Luo, X., Chi, Z., Ji, R., Jiang, H., and Chen, K. (2002) Brownian dynamics simulations of the recognition of the scorpion toxin P05 with the small-conductance calcium-activated potassium channels, *J. Mol. Biol. 318*, 417−428.
68. Moran, O. (2001) Molecular simulation of the interaction of κ-conotoxin-PVIIA with the Shaker potassium channel pore, *Eur. Biophys. J. 30*, 528−536.
69. Cui, M., Shen, J. H., Briggs, J. M., Luo, X. M., Tan, X. J., Jiang, H. L., Chen, K. X., and Ji, R. Y. (2001) Brownian dynamics simulations of interaction between scorpion toxin Lq2 and potassium ion channel, *Biophys. J. 80*, 1659−1669.
70. Shiau, Y. S., Lin, T. B., Liou, H. H., Huang, P. T., Lou, K. L., and Shiau, Y. Y. (2002) Molecular simulation reveals structural determinants of the hanatoxin binding in Kv2.1 channels, *J. Mol. Model. 8*, 253−257.
71. Lou, K. L., Huang, P. T., Shiau, Y. S., and Shiau, Y. Y. (2002) Molecular determinants of the hanatoxin binding in voltage-gated K^+-channel drk1, *J. Mol. Recognit. 15*, 175−179.
72. Huang, P. T., Chen, T. Y., Tseng, L. J., Lou, K. L., Liou, H. H., Lin, T. B., Spatz, H. C., and Shiau, Y. Y. (2002) Structural influence of hanatoxin binding on the carboxyl terminus of S3 segment in voltage-gated K^+-channel Kv2.1, *Recept. Channels 8*, 79−85.
73. Lou, K. L., Huang, P. T., Shiau, Y. S., Liaw, Y. C., Shiau, Y. Y., and Liou, H. H. (2003) A possible molecular mechanism of hanatoxin binding-modified gating in voltage-gated K^+-channels, *J. Mol. Recognit. 16*, 392−395.
74. Nishizawa, M., and Nishizawa, K. (2006) Interaction between K^+ channel gate modifier hanatoxin and lipid bilayer membranes analyzed by molecular dynamics simulation, *Eur. Biophys. J. 35*, 373−381.
75. Sanchez, R., and Sali, A. (2000) Comparative protein structure modeling. Introduction and practical examples with modeller, *Methods Mol. Biol. 143*, 97−129.
76. Lindahl, E., Hess, B., and van der Spoel, D. (2001) GROMACS 3.0: a package for molecular simulation and trajectory analysis, *J. Mol. Model. 7*, 306−317.
77. van Gunsteren, W. F., and Berendsen, H. J. C. (1987) *Gromos-87 Manual*, Biomos BV, Groningen.
78. van Gunsteren, W. F., Kruger, P., Billeter, S. R., Mark, A. E., Eising, A. A., Scott, W. R. P., Huneberger, P. H., and Tironi, I. G. (1996) *Biomolecular Simulation: The GROMOS96 Manual and User Guide*, Biomos and Hochschulverlag AG an der ETH Zurich, Groningen and Zurich.
79. Hermans, J., Berendsen, H. J. C., van Gunsteren, W. F., and Postma, J. P. M. (1984) A consistent empirical potential for water-protein interactions, *Biopolymers 23*, 1513−1518.
80. Berendsen, H. J. C., Postma, J. P. M., van Gunsteren, W. F., DiNola, A., and Haak, J. R. (1984) Molecular dynamics with coupling to an external bath, *J. Chem. Phys. 81*, 3684−3690.
81. Darden, T., York, D., and Pedersen, L. (1993) Particle mesh Ewald−an N.log(N) method for Ewald sums in large systems, *J. Chem. Phys. 98*, 10089−10092.
82. Essmann, U., Perera, L., Berkowitz, M. L., Darden, T., Lee, H., and Pedersen, L. G. (1995) A smooth particle mesh Ewald method, *J. Chem. Phys. 103*, 8577−8593.
83. Hess, B., Bekker, H., Berendsen, H. J. C., and Fraaije, J. G. E. M. (1997) LINCS: A linear constraint solver for molecular simulations, *J. Comput. Chem. 18*, 1463−1472.
84. Miyamoto, S., and Kollman, P. A. (1992) Settle−an analytical version of the Shake and Rattle algorithm for rigid water models, *J. Comput. Chem. 13*, 952−962.
85. Humphrey, W., Dalke, A., and Schulten, K. (1996) VMD−visual molecular dynamics, *J. Mol. Graphics 14*, 33−38.
86. Vriend, G. (1990) WhatIf−a molecular modeling and drug design program, *J. Mol. Graphics 8*, 52−56.
87. Tristram-Nagle, S., and Nagle, J. F. (2004) Lipid bilayers: thermodynamics, structure, fluctuations, and interactions, *Chem. Phys. Lipids 127*, 3−14.
88. Eisenberg, D., Schwarz, E., Komaromy, M., and Wall, R. (1984) Analysis of membrane and surface protein sequences with the hydrophobic moment plot, *J. Mol. Biol. 179*, 125−142.
89. Killian, J. A., and von Heijne, G. (2000) How proteins adapt to a membrane-water interface, *Trends Biochem. Sci. 25*, 429−434.
90. Swartz, K. J., and Mackinnon, R. (1997) Hanatoxin modifies the gating of a voltage-dependent K^+ channel through multiple binding sites, *Neuron 18*, 665−673.
91. Lee, M. S., Salsbury, F. R., and Brooks, C. L. (2004) Constant-pH molecular dynamics using continuous titration coordinates, *Proteins: Struct., Funct., Bioinf. 56*, 738−752.
92. Nielsen, S. O., Lopez, C. F., Srinivas, G., and Klein, M. L. (2004) Coarse grain models and the computer simulation of soft materials, *J. Phys.: Condens. Matter 16*, R481−R512.

93. Lopez, C. F., Nielsen, S. O., Ensing, B., Moore, P. B., and Klein, M. L. (2005) Structure and dynamics of model pore insertion into a membrane, *Biophys. J. 88*, 3083−3094.
94. Bond, P. J., and Sansom, M. S. P. (2006) Insertion and assembly of membrane proteins via simulation, *J. Am. Chem. Soc. 128*, 2697−2704.
95. Hénin, J., Pohorille, A., and Chipot, C. (2005) Insights into the recognition and asscoiation of transmembrane α-helices. The free energy of α-helix dimerization in glycophorin A, *J. Am. Chem. Soc. 127*, 8478−8484.

BI061111Z